INVESTIGATION OF A TWIN ENTRY MIXED FLOW TURBINE VOLUTE, BENEFITS WITH REGARD TO THE ECO-SYSTEM

M. Hamel[1*], M.M. Bencherif[1], M. K. Hamidou[1]

[1]Laboratory of Applied Mechanics, Faculty of Mechanical Engineering, University of Science and technology Mohamed Boudiaf, BP-1505Oran El M'Naouer, Algeria

*e-mail: mohammed.hamel@univ-usto.dz

Abstract. Mixed-inflow turbines are suitable for many applications, where compact power sources are required with higher boost pressure. Realizing the growing importance and availability of road vehicles operating over wide range of speeds and loads, our point of particular interest must be a reduction of gas pollutants which could be achieved by exploring different design possibilities in order to increase the machine efficiency. This will certainly lead to a decrease in fuel consumption resulting in a fall of C02 gas emission amount. This paper focuses on the performance predictions of a turbocharger Twin-entry mixed inflow turbine. The ANSYS-CFX code is used to solve the equations of a viscous, compressible, turbulent, highly unsteady and three dimensional turbine inflow. The computed results agree reasonably well with experimental data. Twin-entry turbine provides the best compromise in terms of performances at different pressure ratio, and significant increase in swallowing capacity probably due to the better flow guidance, a more uniform thermodynamic parameters and Mach number around the rotor inlet.

1. Introduction

Fuels for motor vehicles other than gasoline are being eyed because they generated lower levels of pollutants than does gasoline, since if the CO2 content of the combustion products rises above 15% it would be harmful to the health. It should be emphasized that turbocharged internal combustion engines work with a higher air/fuel ratio for less toxic gas emissions and resulting in significantly increase in the specific power output, both features represent attractive accomplishments.. A study of CO2 emissions of different end-use sectors in the United States in 2008 conducted by the US Environmental Protection Agency [1] showed approximately 32% of CO2 emissions are from the transportation sector, and almost entirely from fossil fuel combustion. Carla et al [2] focuses on exploiting ways to reduce fuel consumption and emissions from gasoline road vehicles, with turbocharging mechanisms, and the combination of the three cheapest and low-complexity mechanisms (fuel cut, stop–start and downsizing with turbocharging), fuel consumption and CO2 emissions can be reduced by 15–49%.The effects of the engine exhaust system as well as the influence of turbocharging have been studied extensively, as reported at [3]. The performance of lean-burn stationary engines fueled by natural gas has been investigated by Klimstra J. [4] the results show that limitations for the NOx emissions restrict the developments in cylinder load and shaft efficiency. Opportunities exist for decreasing the CO and HC emissions. The effect of the turbocharging system on the performance of the gas engine family, which is used in combined power plants, is investigated by Ugur [5], the results show that the turbocharger efficiency has a great influence on the engine

efficiency. An increase of 1% in the turbocharger efficiency brings an increase of around 0.08% in the engine efficiency.

The volute is an essential element in the centrifugal machines. Improving the performance of a volute is an effective way to improve the total performance of the machine.

For this purpose, it is of interest to compare effect and benefits between a single-entry and a twin-entry volute in terms of thermodynamic parameter uniformity, maximum kinetic energy, appropriated incidence angle to the rotor and minimum losses. The twin-entry mixed inflow turbine is investigated under highly pulsating unfavorable flow. It is fortunate that the turbine is able to accept these conditions without a complete deterioration of its performance.

There are several experimental investigations on the single entry mixed inflow turbine performance. Three mixed flow turbines, with rotor A, B and C, have been designed to meet the above mentioned constrains and then tested at Imperial College by Abidat [6] and Abidat et al. [7], the two rotors A and C have a 20 degrees constant rotor inlet blade angle and differ only by the number of blades: Rotor A has 12 blades while turbine C has only 10. An experimental campaign developed on a turbocharger waste-gated turbine for gasoline engine application is presented by Vincenzo et al [8]. Chen et al. [9] study the effect of pulse amplitude and frequency on the mixed flow turbine. The performance of mixed flow turbine with different rotors has been investigated by Arcoumanis et al. [10]. The steady and unsteady performances of two mixed flow turbocharger turbine rotors has been presented by Hakeem et al. [11], a detailed assessment of the influence of volute geometry on the turbine performance has been carried out, which confirmed that the geometry of volute plays a critical role in the overall performance of a turbine. Abidat et al. [12] proposed a method to predict the performance of a mixed flow turbine under both steady and unsteady conditions. Hamel et al. [13] study the influence of the volute inlet flow conditions on its performance (efficiency, exit flow angle, etc). Hamel et al. [14] for steady and unsteady flow performance analyses and a numerical performance prediction of a mixed flow turbine under inlet pulsating flow conditions in addition, the influence of the pulse frequency is studied.

Twin entry turbochargers have been widely used in industry for large-size engines, but limited research has been undertaken for medium-sized engines. Therefore, more studies are necessary to provide further insights into the key benefits, in adopting a twin-entry turbocharger. Almost most of the researches in this area are experimental. Aghaali et al. [15] carried out experimental measurements on twin-entry turbine and the results showed that the two entries appeared to be significantly different in terms of mass flow rate and efficiency characteristics. Experimental results of Hajilouy et al. [16] show that the maximum efficiency occurs at equal admission for the considered range. Meanwhile, the lowest efficiency occurs when the whole flow is in hub side entry. Rajoo et al. [17] discussed the performance analysis of a twin-entry variable geometry turbine with rotor tested in Imperial College London under pulsating flow conditions. Payri et al. [18] proposed a physical model to calculate the fluid dynamic behaviour and energy conversion of a single-entry turbine and a twin-entry turbine. Chiong et al. [19] developed five one-dimensional models of increasing complexity to study the geometrical effects on flow under full admission.

The ANSYS-ICEM tool is used to build the full turbine geometry and to generate the mesh while computational tests are performed with the ANSYS-CFX code. The steady and unsteady flow both are characterized by a pressure ratio range between 1.9 and 3.3 at 100% equivalent design speed (59 740 rpm) and inlet total temperature of 342.2˚K.The numerical simulation results on the single and twin-entry volute of mass flow rate, total to static efficiency both versus pressure ratio, pressure distribution along the axial distance are compared to experimental data. The predicted volute efficiency function of the expansion ratio, the absolute outlet flow angle from the volute, the Mach number and the pressure distribution on azimuth positions from the volute outlet are presented. The swallowing capacity under unsteady regime

is obtained for the single and twin-entry volute, characterized by the Dale's loop, a double loop in the twin-entry case is observed. Studies are necessary to provide further insight into the key benefits, otherwise, of adopting a twin-entry turbocharger as shown in this study.

2. Flow simulations in a mixed inflow turbine

Mixed Inflow geometry. The turbine wheel under investigations is a mixed inflow type, with constant blade angle (named rotor A at the laboratory of Imperial College),a volute cross section area as show in Fig. 1 designed at the Imperial College. The main geometrical parameters are given in Table 1. The volutes of the twin -entry turbine and the single-entry turbine have the same area and radius center of the cross section. Because of the non-symmetry of the single-entry volute cross section, it can't be divided into two equal parts with respect to the center line radius. Therefore, to obtain one part of an equivalent twin entry volute section, the shape of the single entry volute cross section and center line radius are conserved and the cross section area is divided by two. The second part is obtained by symmetry and a space of 1 mm is left between the two parts of the volute. The section or subsection title have no dot after it; after going text starts from the new line without the intend. The first lines of the following paragraphs should have ½ inch intend from the left side.

Table 1. Turbine geometry.

Volute inlet area	2.12×10^{-3} m2
Volute inlet radius	82.50×10^{-3} m
Rotor inlet mean diameter	83.58×10^{-3} m
Rotor inlet blade height	17.99×10^{-3} m
Rotor inlet blade angle	20.0◦
Rotor inlet cone angle	40.0◦
Exducer hub diameter	27.07×10^{-3} m
Exducer shroud diameter	78.65×10^{-3} m
Rotor exit mean blade angle	−52.0◦
Rotor axial length	40.00×10^{-3} m
Number of blades	12
Radial and axial tip clearance	0.40×10^{-3} m

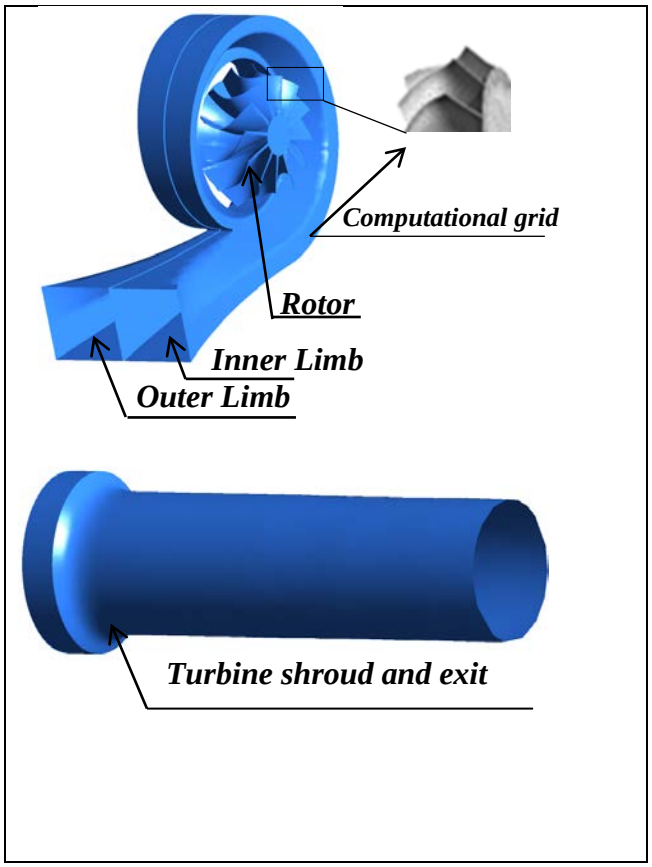

Fig. 1. Mixed flow turbine casing.

Turbulent flow model. The highly three-dimensional flow in the mixed flow turbine is obtained by solving numerically the compressible Reynolds Averaged Navier Stokse (RANS) equations. The turbulence is modeled by the standard $\kappa - \varepsilon$ model. This model is based on the eddy viscosity concept which assumes that the Reynolds stresses $-\rho\overline{u_i u_j}$ *c*an be expressed in terms of the mean velocity gradients and the eddy or turbulent viscosity μ_t in a manner analogous to the viscous stresses τ_{ij} for laminar Newtonian flows.

• Continuity equation:

$$\frac{\partial \rho}{\partial t} + \nabla \bullet \left(\rho \vec{U}\right) = 0, \tag{1}$$

where ρ and $\vec{U}$ are the density and the mean velocity vector respectively.

• Momentum equations

$$\frac{\partial (\rho \vec{U})}{\partial t} + \nabla \bullet \left(\rho \vec{U} \otimes \vec{U}\right) = -\nabla P' \bullet \left(\mu_{eff}\left(\nabla \vec{U} + \left(\nabla \vec{U}\right)^T\right)\right) + S_M, \tag{2}$$

where S_M the sum of the body forces, and μ_{eff} is the Effective Viscosity defined by:

$$\mu_{eff} = \mu + \mu_t, \tag{3}$$

where

$$\mu_t = \rho C_\mu \frac{\kappa^2}{\varepsilon} \tag{4}$$

And P' is a modified pressure, defined by:

$$P' = P + \frac{2}{3}\rho\kappa + \frac{2}{3}\mu_{eff}\frac{\partial U_\kappa}{\partial \chi_\kappa}, \tag{5}$$

where $\vec{U}, P, \delta, \tau, -\rho\overline{U_i U_j}$ and S_M are the fluctuating velocity vector, the pressure, the Kronecker delta symbol, the molecular stress tensor, the Reynolds stress tensor and a source term respectively. The Coriolis and centrifugal forces are included in the source term.

• Energy equation:

$$\frac{(\partial \rho H)}{t} + \nabla \bullet \left(\rho \vec{U} H - \rho \overline{\vec{u}h} - \lambda \nabla T\right) = \frac{\partial P}{t} \quad (6)$$

In this equation, H is the mean total enthalpy given by:

$$H = h_s + \frac{1}{2}\vec{U}^2 + \kappa, \quad (7)$$

where h_s is the mean static enthalpy, λ is the thermal conductivity, T is the mean static temperature and the additional term k in the total energy equation is the turbulent kinetic energy defined as follows:

$$\kappa = \frac{1}{2}\vec{u}^2 \quad (8)$$

Static temperature, static pressure p and density ρ are related by the equation of state: $p = \rho RT$, where R is the air gas constant.

We define the reduced mass flow rate:

$$\dot{m}_r = 10^5 \dot{m} \sqrt{T_{0^*}/P_{0^*}} \quad (9)$$

The expansion ratio:

$$P_r = P_{0^*}/P_4 \quad (10)$$

And the total to static efficiency

$$\eta_{ts} = (h_{0^*} - h_4)/cpT_{0^*}[1 - (P_4/P_0)]^{(\gamma-1)/\gamma} \quad (11)$$

The $\kappa - \varepsilon$ model assumes that the eddy viscosity μ_t is linked to the turbulent kinetic energy κ and its dissipation rate ε through the following relation:

$$\mu_t = \rho C_\mu \frac{\kappa^2}{\varepsilon}, \quad (12)$$

where C_μ = 0.09 and κ and ε are defined through the following two equations:

$$\frac{\partial(\rho k)}{\partial t} + \nabla(\rho U K) = \nabla\left[\left(\mu + \frac{\mu_t}{\sigma_k}\right)\nabla K\right] + P_\kappa - \rho\varepsilon \quad (13)$$

$$\frac{\partial(\rho \varepsilon)}{\partial t} + \nabla(\rho U \varepsilon) = \nabla\left[\left(\mu + \frac{\mu_t}{\sigma_\varepsilon}\right)\nabla \varepsilon\right] + \frac{\varepsilon}{K}(C_{\varepsilon 1} P_K - C_{2\varepsilon}\rho\varepsilon) \quad (14)$$

In this model, P_K is the turbulence production and the flowing constants are determined experimentally from a wide range of turbulent flows (Patankar and Spalding [20]) $\sigma_\kappa = 1.00$, $\sigma_\varepsilon = 1.30$, $C_{1\varepsilon} = 1.44$, $C_{2\varepsilon} = 1.92$.

Modeling the flow near the wall. The flow near the wall is modeled with the use of the scalable wall function formulation. The idea behind the scalable wall function is to avoid the limitations imposed by standard wall functions in terms of near-wall grid resolution. If the boundary layer is not fully resolved, it will be relying on the logarithmic wall function approximation to model the boundary layer. Assuming that the logarithmic profile reasonably approximates the velocity distribution near the wall, it provides a means to compute numerically the fluid shear stress as a function of the velocity at a given distance from the wall Equation (15).

$$\tau_w = \rho u_\tau^2, \quad (15)$$

where the friction velocity u_τ is given by the logarithmic relation for the near wall velocity:

$$u_\tau = \frac{U_t}{\frac{1}{0.41} log(\tilde{y}^+) + 5.2} \quad (16)$$

In this equation, U_t is the known velocity tangent to the wall at a normal distance of Δ_y from the wall and $\tilde{y}^+ = max(y^+, y^+_{lim})$, where $y^+ = \rho u_\tau \Delta y/\mu$. The limiting value of $y_l im^+ = 11.067$ marks the intersection between the logarithmic and the linear profile.

The y^+ limiter prevents the formulation to become singular as y^+ tends to 0 and to switch to a linear relationship between u_τ and U_t if the first grid point is not located in the logarithmic part of the boundary layer.

3. Numerical method

The integration, on the finite volumes, of the equations describing the turbulent flow, results in a set of discrete equations. The terms of the differential equations on the volume interfaces are obtained by a first order upwind scheme or a high resolution (second order upwind scheme). The first order upwind scheme – which is more robust than higher order schemes – is generally used to obtain an approximate solution of the flow while the high resolution scheme is used to obtain the final solution. The simulation with first order scheme is initialized using linear interpolation between boundary condition quantities and then the solution is used as an initial guess for the final simulation. This ensures a relatively rapid convergence.

The ANSYS-CFX code uses a single cell, collocated grid to overcome the decoupling of pressure and velocity. The method is similar to that used by Rhie and Chow [21], with a number of extensions to achieve numerical solutions that are independent of both the under relaxation factor and the time step size of the steady-state solution. The method improves the robustness of the discretization when the pressure varies rapidly or is affected by body forces.

The pressure–velocity coupling is achieved using a coupled solver, which solves the hydrodynamic equations (for u, v, w, p) as a single system. This solution approach uses a fully implicit discretization of the equations at any given time step. At the domain inlet, the flow is assumed subsonic, and therefore the total pressure, the total temperature and a medium intensity of turbulence (5%) in the stationary frame of reference as well as the flow direction are imposed. The turbulence quantities at the inlet boundary are obtained from the inlet hydraulic diameter and the intensity of turbulence. At the turbine outlet, where the flow is considered to be subsonic, the mass flow rate is imposed. On the solid boundaries, a no slip condition is used.

4. Mesh generation

The flow solution in the mixed flow turbine, shown in Fig. 2, is obtained by a numerical finite volume method. The flow domain is discredited into finite volumes of tetrahedral elements and prism elements in the near wall layer. The ICEM CFD software tool is used to build the turbine geometry and to generate the unstructured mesh. The main geometrical characteristics of the mixed flow turbine are given in Table 1.

The single entry and twin entry turbine geometries are split into a stationary volute part (42085 and 317564 nodes, 144546 and 790872 elements) and a rotating rotor part (120600 and 145173 nodes, and 449864 and 548684 elements) respectively. A view of the grids on the surfaces of the main turbine parts is shown below.

During the mesh generation process, care has to be taken when choosing the first grid spacing near wall boundaries to obtain a proper resolution of the boundary layer. As a result of the use of the wall function approach to model the flow near the wall in the RNG $k-\varepsilon$ turbulence model, it is advised that the y^+ value for the near wall nodes has to be in the range of 20 to 100.

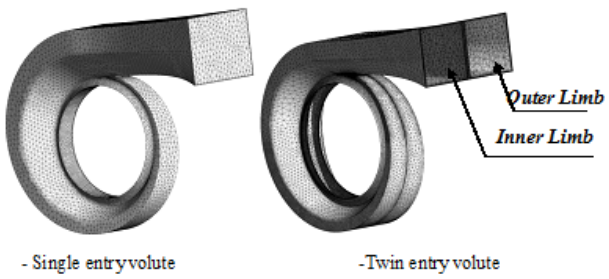

Fig. 2. Computational grid of the mixed flow turbine.

5. Results and discussion

Steady, equal admission. The steady state performance characteristics of the volute twin-entry and the single-entry mixed turbine are investigated. The steady simulation for equal

admission swallowing capacity data is performed at constant speed with a varying pressure ratio in a range of 1.9 to 3, 3 at 100% of relative speed, which corresponded to a shaft speed of 59,740 rpm at full admission conditions and an inlet total temperature of 342.2˚K.With the above imposed conditions of operation, the mass flow rate and the total to static efficiency both versus the expansion ratio (Pr), and the pressure distribution along the axial distance are presented on Fig. 3, Fig. 4 and Fig. 5 respectively, compared to the experimental curve obtained from a turbo compressor test rig at Imperial College by Abidat et al [3]. A good agreement between estimated and experimental results is obtained for a wide range of pressure and axial distance. Experimental measurement of mass flow rate has almost the same trend with a difference of 4% for the turbine with single-entry and 2.3% for the turbine with a twin-entry volute. The mass flow rate in the twin-entry volute is slightly lower compared to the single entry turbine in the steady case, this difference might be due to the additional surface of fluid contact (separation surface between the inner limb and outer limb).

Although, the wall friction losses in the case of a twin-entry volute are expected to be greater than the case of single-entry due to a larger surface of contact, the curve of twin-entry efficiency reveals little larger values and approaching the experiment points. The maximum discrepancy is of the order 3.75 %.

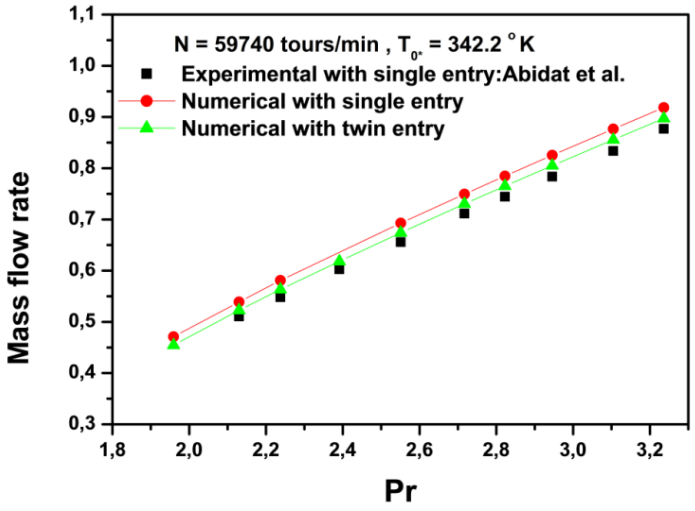

Fig. 3. Predicted and experimental steady results of mass flow rate vs. pressure ratio.

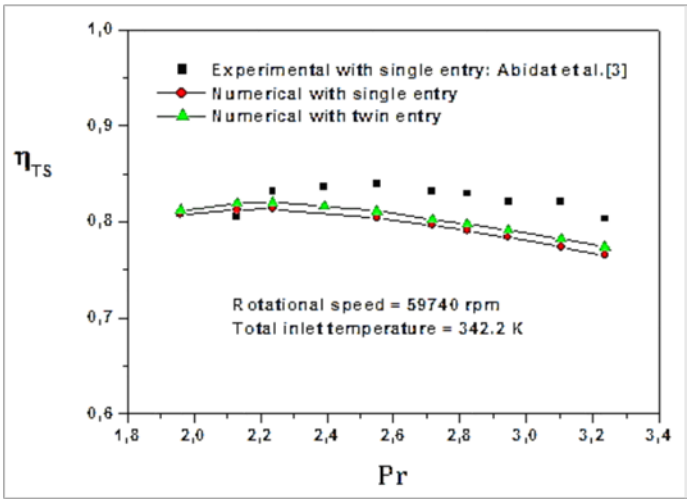

Fig. 4. Predicted and experimental results of the turbine efficiency vs. pressure ratio.

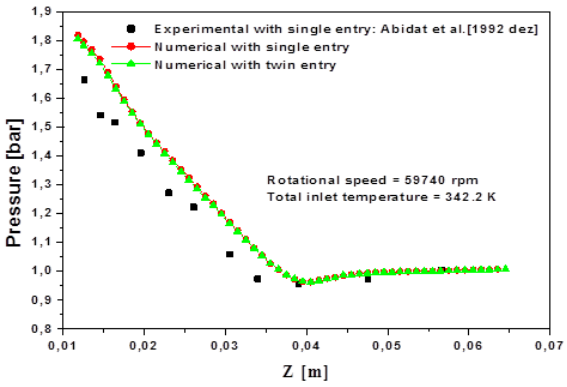

Fig. 5. Predicted and experimental results of the pressure distribution vs. Axial distance.

The contours of exit flow angle at the rotor entry (volute exit) for three different values of pressure ratio are shown in (Fig. 6), this angle corresponds to the full admission .The large positive angle value is remarked on the volute twin-entry and the negative flow angle is observed in the single-entry volute. The wake region in this type of volute is less than in a symmetrical one, because of the inclined shroud side entry in which the flow enters the wake region directly and destroys it. Another point is the deviation of flow from the radial plane that attempts to decrease it by making volute in asymmetrical form, therefore, the flow angle at the rotor inlet with the single-entry volute is circumferentially non uniform.

In Fig. 7, the variations of Mach number from the volute inlet to the outlet are depicted at three different pressure ratios (1.95, 2.55 and 3.23), while (Fig. 8) show the pressure distribution in the rotor inlet, an acceleration of the flow from the inlet to the outlet of the single and the twin-entry volute, this acceleration is greater in the twin-entry volute than to the single-entry volute. The pressure and the Mach number distribution is more uniform and smoother for the twin-entry volute compared to single-entry volute, which is a result of the stationary inlet pressure. The more uniform and smoother pressure distribution for the twin-entry volute case in the wheel implies that the twin-entry turbine can extract more energy out of the gas uniformly distributed at the rotor.

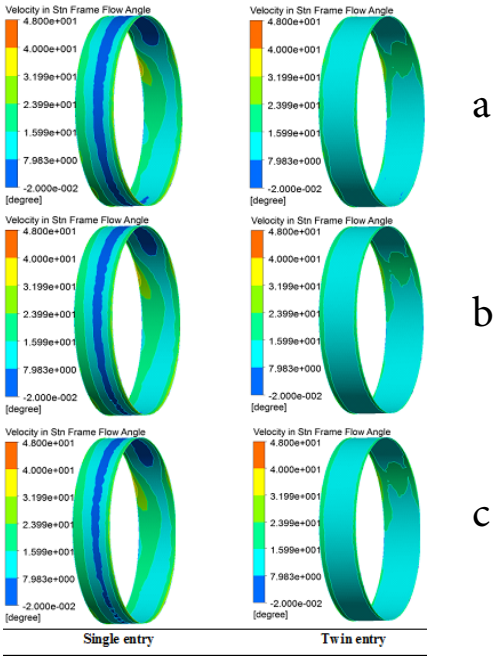

Fig. 6. Variation of flow angle at the volute outlet
(a - Pr = 1.95; b - Pr = 2.55; c - Pr = 3.23).

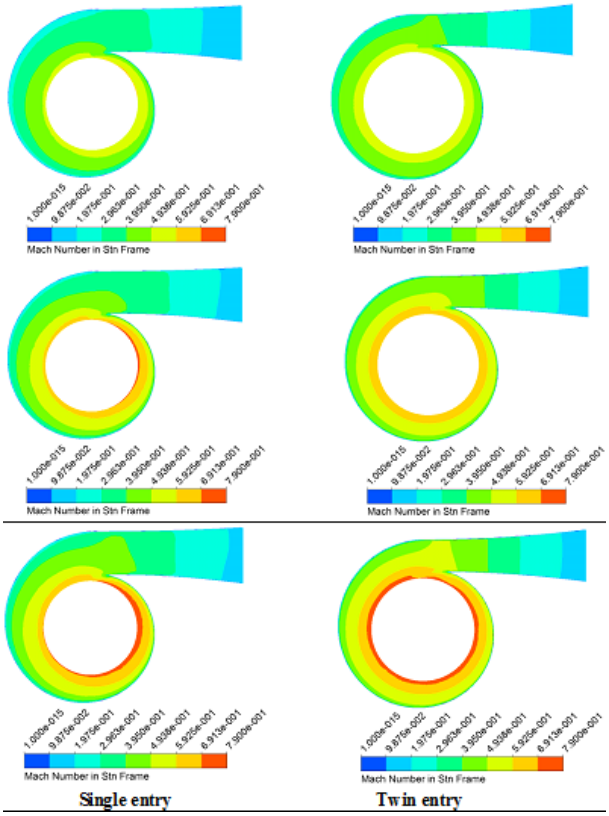

Fig. 7. Variation of Mach number from the volute inlet to the outlet of the volute (a - Pr = 1.95; b - Pr = 2.55; c - Pr = 3.23).

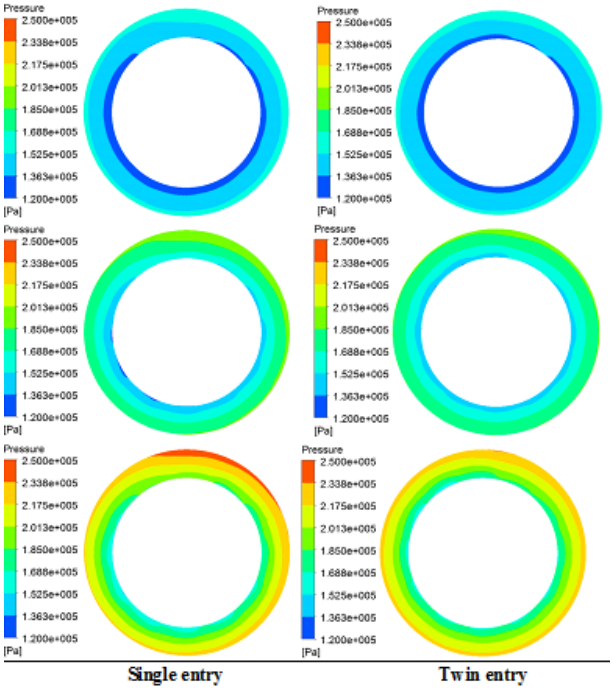

Fig. 8. Variation of the pressure at the volute outlet (a - Pr = 1.95; b - Pr = 2.55; c - Pr = 3.23).

Unsteady flow admission. The Fig. 9 shows a comparison between experimental and computed fluctuating components of the instantaneous turbine power calculated from Equation (17), where the instantaneous turbine power is the product of the instantaneous turbine torque and the angular velocity. Turbine torque is derived by integrating the element torque on each

blade surface while it is obtained experimentally by evaluation of the angular acceleration of the turbocharger turbine and the compressor load. It is probably due to the inertia of the assembly, the compressor load and the variation of the rotational velocity that the computed power trace is shifted from the experimental. The twin-entry configuration produces 3.27% greater power when compared to the single entry. The greatest gain in power output for the twin-entry configuration was observed, this power gain is resultant from the increase in compressor performance due to the improved energy transfer from the exhaust gases to the turbine impeller, therefore adopting a twin-entry turbine housing has clearly improved the torque characteristics.

$$\dot{W}'(t) = \dot{W}(t) - \frac{1}{T}\int_0^T \dot{W}(t)dt \qquad (17)$$

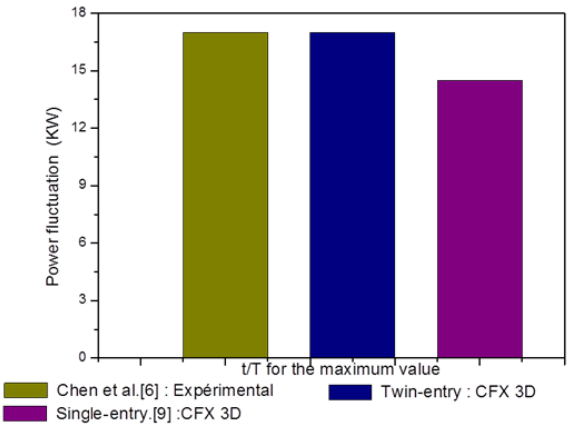

Fig. 9. The predicted power fluctuations.

The figure 10 shows the swallowing capacity of single entry and twin-entry turbine at 50% equivalent speed and 180° out of phase admission, for 40 hz pulsating flow conditions are shown. The calculation of the overall swallowing capacity of the twin-entry turbine is not straightforward in an unequal flow conditions. The pressure ratios of the two entries will reduce the range covered during a cycle, compared to the individual entry, as well as the double looping in the overall swallowing capacity representing both entries, which means the twin-entry turbine exhibits more of a filling and emptying characteristics, consistent with the observed characteristics of the single-entry turbine.

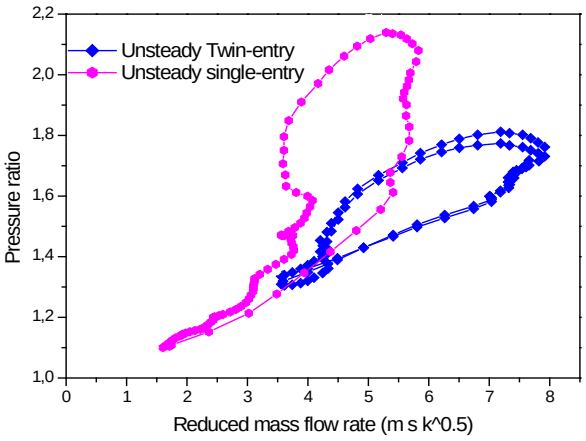

Fig.10. Swal1lowing capacity of single entry and twin-entry turbine at 50% equivalent speed and 180° out of phase admission.

6. Conclusions

We retain from the present study that turbochargers are widely used as a mean of increasing the output power of the machine commonly to road transportation and arise as a case of particular interest suited for less fuel consumption and less pollutant gas emissions. Roughly 30 to 40 percent of the chemical energy released by the combustion is lost in the engine exhaust gas and saved partially in the internal combustion engine cycle with a significant lower outlet temperature to the ambient atmosphere. The above focused echo- system considerations are very sensitive to the machine performances as a whole. A comparative performance estimation is proposed, keeping in mind the eco-system objectives. The twin-entry volute numerical results reveal that in both steady and pulsating flow regimes subsequent thermodynamic parameters and Mach number uniformity is obtained around the rotor inlet, a higher total to static efficiency is maintained also it offers an appropriate absolute flow angle distribution with azimuthally angle, and a larger swallowing capacity is notified which is of prime importance as it affects the turbine output power, when compared to a single entry volute. The calculated total to static efficiency and the mass flow rate versus expansion ratio, the pressure distribution along the axis of the rotation and the power fluctuations are all validated with the experimental available data. The mass flow rate experimental measurements have almost the same trends with a difference of 4% in the case of the single entry turbine and 2.3% for the twin entry turbine. The total to static efficiency simulation results of the twin-entry volute are little bit greater than the single entry volute. The twin-entry configuration achieves a power excess of 3.27 % compared to the single entry volute probably due to a better flow guidance, a more uniform thermodynamic parameters and Mach number around the rotor inlet and a larger swallowing capacity. It is worth commenting that the impact of these improved results on the eco-system should be realistic.

References

[1] Inventory of US Greenhouse Gas Emissions and Sinks: 1990–2008, Executive Summary. EPA report 430-S-10-001; United States Environmental Protection Agency (Office of Atmospheric Programs 6207J; Washington, 2010), http://www.epa.gov/climatechange/emissions/downloads10/US-GHG-Inventory 2010_Executive Summary.pdf (accessed 21.08.11).

[2] Carla Silva, Marc Ross, Tiago Farias // *Energy Conversion and Management* **50(2)** (2009) 215.

[3] N. Watson, MS. Janota, *Turbocharging the internal combustion engine* (The Macmillan Press, 1982). doi:10.1007/978-1-349-04024-7.

[4] J. Klimstra, *Performance of lean-burn natural-gas-fuelled engines–On specific fuel consumption, power capacity and emissions* (SAE Technical Papers, 1990). doi:10.4271/901495.

[5] Ugur Kesgin // *Energy Conversion and Management* **46(1)** (2005) 11. doi:10.1016/j.enconman.2004.02.006.

[6] M. Abidat, *Design and testing of a highly loaded mixed flow turbine,* PhD thesis (Imperial College of Science Technology and Medicine University of London, 1991).

[7] M. Abidat, H. Chen, N.C. Baines // *Proceedings of the Institution of Mechanical Engineers, Part A Journal of Power and Energy* **206(2)** (1992) 95. doi:10.1243/PIME_PROC_1992_206_016_02.

[8] D.B. Vincenzo, M. Silvia, B. Fabio, C. Massimo, // *Energy Procedia* **45** (2014) 909.

[9] H. Chen, I. Hakeem, R.F. Martinez Botas, // *Proceedings of the Institution of Mechanical Engineers, Part A Journal of Power and Energy* **210(5)** (1996) 397. doi:10.1243/PIME_PROC_1996_210_063_02.

C. Arcoumanis, I. Hakeem, R.F. Martinez Botas, L. Khezzar, N.C. Baines, Performance of a mixed flow turbocharger turbine under pulsating flow conditions. In: Proceeding of ASME. Turbo Expo: Power for Land, Sea, and Air (1995) 95-GT-210. doi:10.1115/95-GT-210.
[10] I. Hakeem, C.-C. Su, A. Costall, R.F. Martinez Botas // *Proceedings of the Institution of Mechanical Engineers, Part A Journal of Power and Energy* **221(4)** (2007) 535.
[11] M. Abidat, M. Hachemi, M.K. Hamidou, N.C Baines // *Proceedings of the Institution of Mechanical Engineers, Part A: Journal of Power and Energy* **212(3)** (1998) 173.
[12] M.Hamel, M.K. Hamidou, H.T. Cherif, S.A. Litim, *Design and flow analysis of radial and mixed flow turbine volutes*. In: Proceedings of ASME Turbo Expo Power for Land Sea and Air, (2008) GT2008-50503.
[13] M. Hamel, M. Abidat, S.A. Litim // *Comptes Rendus - Mecanique* **340(3)** (2012) 165. doi:10.1016/j.crme.2012.01.004.
[14] Bowman, M., Debray, S. K., and Peterson, L. L. // *ACM Trans. Program. Lang. Syst* **15(5) (1993)** 795.
[15] H. Aghaali, A. H. Benisi // I*ranian Journal of Science and Technology, Transaction B: Engineering* **32(6)** (2008) 571.
[16] A. Hajilouy, M. Benisi, M. Rad, R. Shahhosseini // Archive of *Applied Mechanics* **79(12)** (2009) 1127.
[17] S. Rajoo, R. Alessandro, R.F. Martinez-Botas // *Energy* **38 (1)** (2012) 176.
[18] F. Payri, J. Benajes, M. Reyes // *International Journal of Mechanical Sciences* **38(8-9)** (1996) 853.
[19] M.S. Chiong, S. Rajoo, R.F. Martinez-Botas, A.W. Costall // *Energy Conversion and Management* **57** (2012) 68. doi:10.1016/j.enconman.2011.12.001
[20] S.V. Patankar, D.B. Spalding // *International Journal of Heat and Mass Transfer* **15(10)** (1972) 1787.
[21] C.M. Rhie, W.L.A. Chow // AIAA Journal **20(11)** (1982) 1525